micromachines

MDPI

Article

High Oxygen Sensitivity of TiO_2 Thin Films Deposited by ALD

Aleksei V. Almaev [1,2,*], Nikita N. Yakovlev [1], Dmitry A. Almaev [1], Maksim G. Verkholetov [1,3], Grigory A. Rudakov [3] and Kristina I. Litvinova [3]

1 Research and Development Center for Advanced Technologies in Microelectronics, National Research Tomsk State University, 634050 Tomsk, Russia; nik_mr_x@mail.ru (N.N.Y.); almaev001@mail.ru (D.A.A.); verkhmaks@yandex.ru (M.G.V.)
2 Fokon LLC, 248035 Kaluga, Russia
3 Institute of Nanotechnology of Microelectronics of the Russian Academy of Sciences, 119991 Moscow, Russia; rudakov.g@inme-ras.ru (G.A.R.); litvinova@misis.ru (K.I.L.)
* Correspondence: almaev_alex@mail.ru; Tel.: +7-923-437-0833

Abstract: The gas sensitivity and structural properties of TiO_2 thin films deposited by plasma-enhanced atomic layer deposition (ALD) were examined in detail. The TiO_2 thin films are deposited using Tetrakis(dimethylamido)titanium(IV) and oxygen plasma at 300 °C on SiO_2 substrates followed by annealing at temperatures of 800 °C. Gas sensitivity under exposure to O_2 within the temperature range from 30 °C to 700 °C was studied. The ALD-deposited TiO_2 thin films demonstrated high responses to O_2 in the dynamic range from 0.1 to 100 vol. % and low concentrations of H_2, NO_2. The ALD deposition allowed the enhancement of sensitivity of TiO_2 thin films to gases. The greatest response of TiO_2 thin films to O_2 was observed at a temperature of 500 °C and was 41.5 arb. un. under exposure to 10 vol. % of O_2. The responses of TiO_2 thin films to 0.1 vol. % of H_2 and 7×10^{-4} vol. % of NO_2 at a temperature of 500 °C were 10.49 arb. un. and 10.79 arb. un., correspondingly. The resistance of the films increased due to the chemisorption of oxygen molecules on their surface that decreased the thickness of the conduction channel between the metal contacts. It was suggested that there are two types of adsorption centers on the TiO_2 thin films surface: oxygen is chemisorbed in the form of O^{2-} on the first one and O^- on the second one.

Keywords: TiO_2 films; atomic layer deposition; gas-sensitive properties; oxygen sensors; sensory effect

check for updates

Citation: Almaev, A.V.; Yakovlev, N.N.; Almaev, D.A.; Verkholetov, M.G.; Rudakov, G.A.; Litvinova, K.I. High Oxygen Sensitivity of TiO_2 Thin Films Deposited by ALD. *Micromachines* **2023**, *14*, 1875. https://doi.org/10.3390/mi14101875

Academic Editors: Elena Kalinina and Nam-Trung Nguyen

Received: 12 September 2023
Revised: 27 September 2023
Accepted: 28 September 2023
Published: 29 September 2023

1. Introduction

Oxygen is the most important gas for human life, and there is a widespread demand for O_2 sensors and for measuring the O_2 concentration in ambient environment. Oxygen detection at an over 1 vol. % level with a high accuracy is essential to control the reactive chemical concentration in the chemical industry and metallurgy [1] and to analyze exhaust gas composition of automobile engines [2,3].

TiO_2 belongs to the large material class of metal oxide semiconductors [4–10]. It is attractive for developing O_2 sensors due to its low cost and high chemical and thermal stability [11–21]. Now, commercial O_2 sensors are based on bulk and thick-film TiO_2 structures [6]. Such structures are not highly sensitive to O_2. A well-known method for optimizing gas-sensitive properties of materials is the use of thin film structures [16]. Film thickness d plays a key role in the gas sensitivity of thin film structures. It has been shown that the optimal thickness of TiO_2 films providing a high gas sensitivity should be comparable to the Debye length L_D. The L_D = 10–50 nm for TiO_2 at an electron concentration of $n = 10^{16}$–10^{18} cm^{-3} and a permittivity of ε_0 = 18.9. Atomic layer deposition (ALD) is a highly promising method for growing very thin TiO_2 films (d = 10–50 nm) with large homogeneity and reproducibility of structural and electrical properties. The ALD allows deposition of continuous films with high precision control over thickness and impurities levels [21,22].

Previously, the ALD method was used to produce thin films structures of various metal oxide semiconductors, mainly based on SnO_2 (see Table 1). At the same time, the gas-sensitive properties of such structures were studied under the exposure to low concentrations of toxic gases and H_2. Detailed studies on the O_2 sensitivity of ALD-deposited metal oxide films have not been practically carried out. Therefore, the purpose of this work is to gain a deep insight into the gas-sensitive properties of the ALD-TiO_2 thin films under O_2 exposure and to explain them by proposing a theoretical model.

Table 1. Comparison of gas-sensitive characteristics of ALD-deposited metal oxide thin films.

Material	*d* (nm)	Gas	c_g (ppm)	*T* (°C)	*S* (arb. un.)	Ref.
TiO_2	50	NH_3	100	350	4.24	[21]
CNT/TiO_2	10 (TiO_2)	NO_2	8	150	~10	[23]
SnO_2	17.5	C_2H_5OH	500	300	1.64	[24]
SnO_2	10	CO	10^4	450	~21	[25]
WO_3 Ga_2O_3 Ga_2O_3/WO_3	6.5 1.5 1.5/6.5	C_2H_5OH	100	275	~14 ~1.4 ~3.5	[26]
SnO_2	90	H_2	1000	400	~380	[27]
TiO_2/SnO_2 QDs	30 (TiO_2)	CO	1	300	1.8	[28]
SnO_2 In_2O_3/SnO_2	4.4 4/4.4	C_2H_5OH	200	400 350	20 37	[29]
IGZO	150	NO_2	100	200	5154	[30]
ZnO/SnO_2 NSs	24 (ZnO)	HCHO	20	200	38.2	[31]
Fe_2O_3/SnO_2 NShs	20 cycles	HCHO	20	220	4.57	[32]
p-TiO_2	70	NO	10	*RT*	1.244	[33]
P3HT/ZnO NWs	-	NH_3	5	*RT*	1.35	[34]

In Table 1, c_g is the gas concentration; *T* is the operating temperature; *S* is the response; CNT is the carbon nanotubes; QDs is the quantum dots; IGZO is the indium gallium zinc oxide; NSs is the nanospheres; NShs is the nanosheets; P3HT is the poly(3-hexylthiophene); NWs is the nanowires; and *RT* is the room temperature.

2. Materials and Methods

TiO_2 thin films were fabricated by the plasma-enhanced ALD technique using FlexAL ALD equipment (Oxford Instruments, Abingdon, UK). Thermally oxidized silicon plates (SiO_2/Si) were used as substrates. Tetrakis(dimethylamido)titanium(IV) (TDMAT) $[(CH_3)_2N]_4Ti$ (99.999%) (Sigma-Aldrich, St. Louis, MO, USA) was used as the metal precursor with carrier gas of Ar (99.999%) at a flow rate of 200 cm^3/min. Oxygen inductively coupled plasma (ICP) was used as an oxidizer. The discharge was excited in an oxygen atmosphere (99.999%) by a generator with a frequency of 13.56 MHz and a power of up to 300 W. The PEALD pulse durations were set at 0.8 s for TDMAT injection, 3 s for Ar purge, 3 s for exposure to plasma discharge, and 2 s for Ar purge. The growth rate at a temperature of 300 °C was 0.09 nm/cycle. The thickness of the deposited TiO_2 films was 30 nm. A SENTECH Senduro spectral ellipsometer was used to estimate the thickness and the growth rate of TiO_2 films at measurements in the wavelength range of 320–1800 nm.

The as-deposited TiO_2 thin films were annealed at a temperature of 800 °C in an Ar atmosphere at a pressure of 2 kPa for 30 min. The rates of heating from *RT* to 800 °C and cooling from 800 °C to *RT* were 4 °C/min. The heating and cooling of samples were in an Ar atmosphere at a pressure of 2 kPa.

X-ray diffraction (XRD) was performed to determine the phase composition of the thin films and the crystal lattice parameters. XRD spectra of films were measured in a

2θ scanning mode employing a CuK_a radiation operated at 45 kV and 40 mA. The X-ray source wavelength was 1.5406 Å. The microrelief of the film surface was studied by a Bruker Dimension Icon atomic force microscope (AFM). Cross-sectional images of the annealed samples were examined by a Jeol JEM 2100 PLUS transmission electron microscope (TEM) at an accelerating voltage of 200 kV in a bright field (BF) mode. The elemental composition of the films was determined by the BF-TEM mode by means of a JEOL EX-24261M1G5T energy dispersive X-ray spectroscopy (EDX) analyzer at a beam current of 1 nA.

To investigate the gas-sensitive properties, Pt contacts were deposited on the TiO_2 film surface by means of vacuum deposition through a shadow mask. The plate with the film and contacts was divided into separate samples. The prepared samples were planar metal–semiconductor–metal (MSM) structures on SiO_2/Si substrates (Figure 1). The interelectrode distance was kept at 1 mm. The thickness of the Pt contacts was about 330 nm.

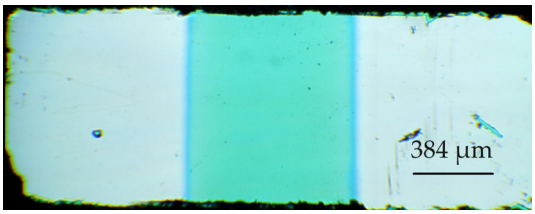

Figure 1. Microscopic photo of the sample based on TiO_2 thin film.

The current–voltage (*I*–*V*) characteristics and time dependences of the sample's resistance under the exposure to various gases were measured by means of a Keithley 2636A source meter and a sealed chamber with a Nextron MPS-CHH micro-probe station. A ceramic-type heater, installed in the sealed chamber, was used to heat the samples from *RT* to 700 °C with a temperature accuracy control of ±0.1 °C. The measurements were carried out under dark conditions and in a flow of dry N_2, or in a gas mixture of dry N_2 + dry O_2. The flow rate of gas mixtures through the measurement chamber was maintained at 500 cm^3/min. A pure dry air or a gas mixture of pure dry air + target gas was pumped through the chamber to examine the selectivity of the samples studied. H_2, CO, CO_2, NO_2, NO and CH_4 were selected as target gases. The source of pure dry air was a special generator. The concentration of the target gas in the mixture was controlled by a gas mixture generator with a Bronkhorst gas mass flow controller. The relative error of the gas flow rate did not exceed 1.5%. The voltage *U* applied to the samples during the measurements of time dependences of the resistance was kept at 3 V.

3. Results and Discussion

3.1. Structural Properties of the ALD-Deposited TiO_2 Thin Films

Figure 2 illustrates a typical XRD spectrum of the annealed ALD-TiO_2 thin film. Several peaks appear at 2θ = 25.3°, 36.9°, 37.8°, 38.2°, 48.0°, 54.0°, 55.1°, 62.7°, 68.8° and 70.3°. These peaks are associated with (101), (103), (004), (112), (200), (105), (211), (204), (116) and (220) Bragg reflections of the tetragonal anatase TiO_2 phase (ICDD 00-021-1272), respectively. These results confirm the polycrystalline nature of the material grown. The wide amorphous halo at 2θ ≈ 22° is due to the SiO_2 layer. The parameters of the tetragonal crystalline lattice of the film are determined as a = 3.78 Å and c = 9.50 Å.

Figure 3 depicts typical annealed ALD-TiO_2 film surface morphology images taken by AFM. The surface roughness parameters of the TiO_2 thin films are R_a = 1.329 nm, R_q = 1.605 nm and R_z = 12.67 nm, where R_a is the arithmetic mean of the absolute values of the deviations of the film surface profile; R_q is the mean square value of the deviations of the film surface profile and R_z is the arithmetic mean of the greatest height of the profile of the film surface. R_q is lower than the value reported in ref. [21] devoted to ALD-deposited TiO_2 thin films. The relatively high surface roughness should lead to an increase in the

surface-to-volume ratio and the surface density of adsorption centers for gas molecules, and, as a result of this, to an increase in responses to gases [35].

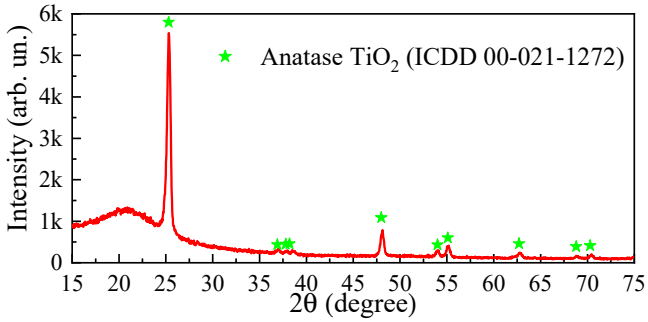

Figure 2. XRD patterns of the ALD-TiO_2 thin films.

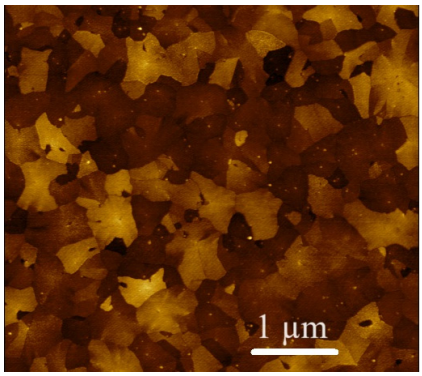

Figure 3. AFM images of annealed ALD-TiO_2 thin film surface.

Figure 4 illustrates a BF-TEM cross-sectional image of annealed ALD-TiO_2 thin film on a substrate in the high-resolution mode. The interplane distance *D* corresponding to the (101) reflection of the anatase TiO_2 phase is 0.353 nm, determined by fast Fourier transformation (FFT). The *D* values for the same plane determined by FFT and by analysis of the XRD pattern (0.352 nm) are the same. TiO_2 thin films have a nanocrystalline structure with amorphous inclusions according to the TEM study.

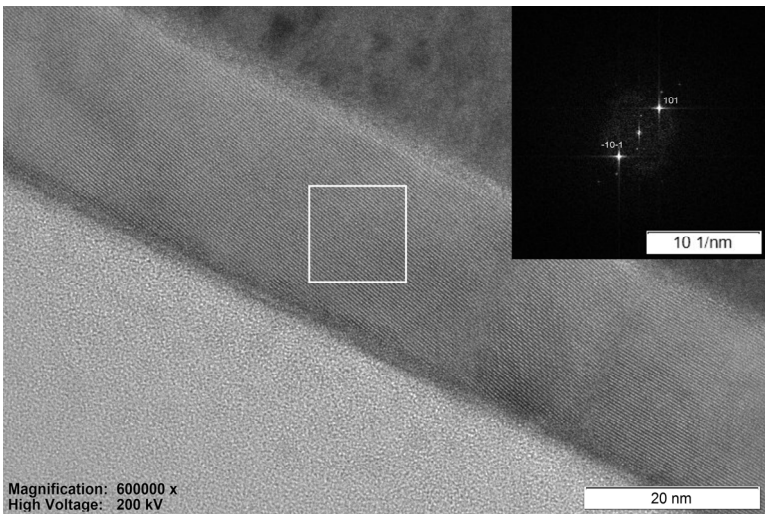

Figure 4. BF-TEM cross-sectional image of annealed ALD-TiO_2 thin film on SiO_2/Si substrate, the insertion is the diffraction pattern.

The contents of Ti and O elements in the films are measured to be ~27 at. % and ~73 at. % (Figure 5a,b), respectively. The increased O content in the films may be associated with features of the ALD process. There is also a peak corresponding to C in the EDX spectrum caused by the technological operations before the measurements of the spectrum.

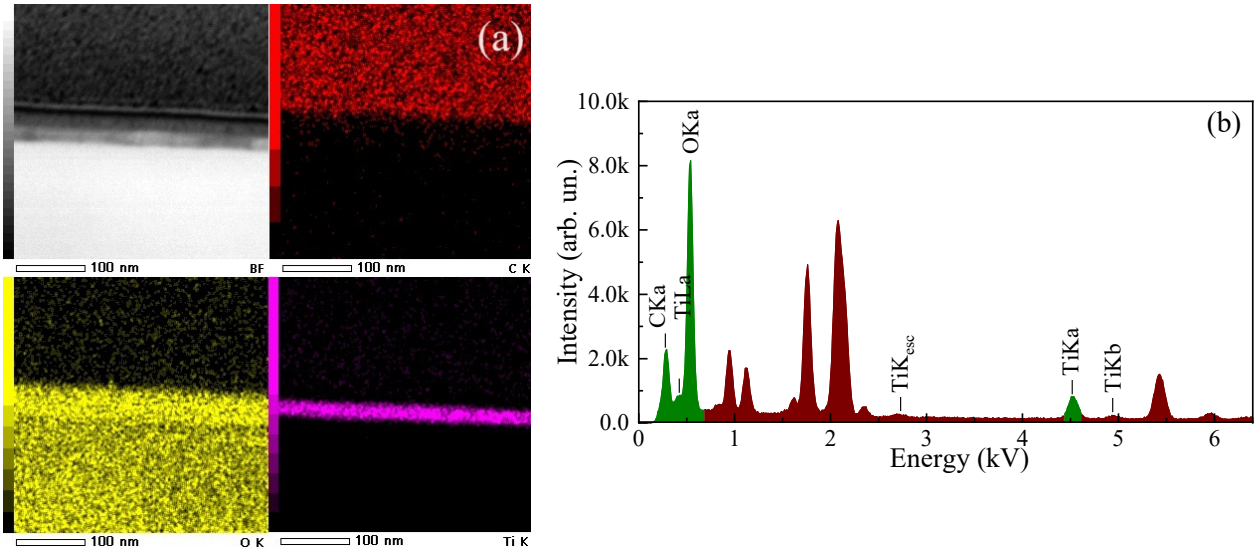

Figure 5. (**a**) Elementwise TEM-EDX mapping of cross-section of annealed ALD-TiO_2 thin film; (**b**) EDX spectrum of annealed ALD-TiO_2 thin film.

3.2. Gas-Sensetive Properties of the ALD-Deposited TiO_2 Thin Films

At the next stage, the gas-sensitive properties of the ALD synthesized TiO_2 thin films were investigated in detail. The exposure to O_2 led to a reversible increase in the resistance of TiO_2 thin films. The following ratio was chosen as the response S_{ox} of samples to O_2:

$$S_{ox} = R_{ox}/R_N, \quad (1)$$

where R_{ox} is the resistance of TiO_2 thin film in a gas mixture of dry N_2 + dry O_2; R_N is the resistance of TiO_2 thin film in dry N_2 atmosphere. The temperature dependencies of the responses under the exposure to 10 vol. % and 40 vol. % of O_2 (Figure 6a) had a maximum at T = 500 °C.

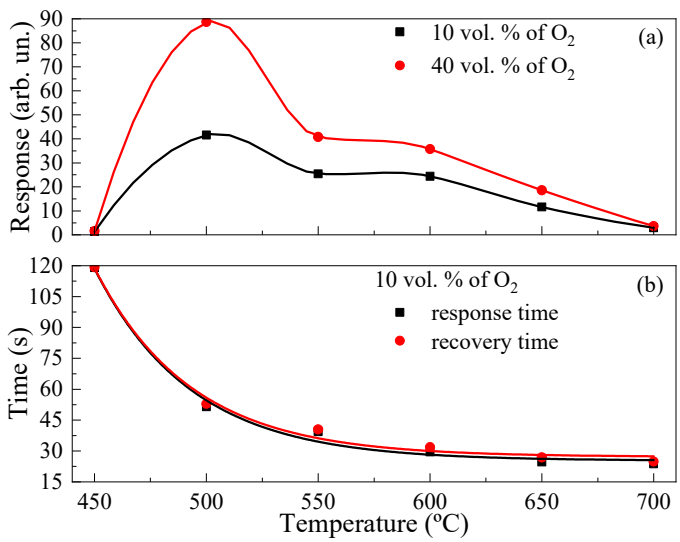

Figure 6. (**a**) Temperature dependences of response to 10 vol. % and 40 vol. % of O_2; (**b**) Temperature dependences of response and recovery times upon exposure to 10 vol. % of O_2.

The samples practically did not react when exposed to O_2 and had a high resistance, making it impossible to reliably register the response to gases at $T < 450$ °C. The presence of a maximum on the temperature dependence of the response is due to the influence of temperature on the processes of dissociation, adsorption/desorption of O_2 molecules, and is specific to metal oxide semiconductors [36,37]. The response t_{res} and recovery t_{rec} times were determined upon exposure to 10 vol. % of O_2 according to the method described in ref. [38] to estimate the operation speed of the films studied. The obtained values of t_{res} and t_{rec} can only be used to compare the operation speed of sensors under similar experimental conditions. We note that the t_{res} and t_{rec} decrease exponentially with the increase in T (see Figure 6b). It is also worth noting that t_{res} and t_{rec} were practically the same at T = 450–700 °C. The t_{res} and t_{rec} did not exceed 30 s in the range of T = 600–700 °C. The t_{res} and t_{rec} were 51.5 s and 52.9 s, respectively, at temperature of the maximum response to O_2.

R_{ox} and R_N decreased by 4% and 36%, correspondingly, during a cyclic exposure to 10 vol. % of O_2 (five cycles) (illustrated in Figure 7a); as a result, S_{ox} increased by 50%. On the other hand, the response of the films to O_2 decreased by 6–7 times during storing in a sealed box at *RT* after the experiments at high T (Figure 7b) mainly due to a significant increase in R_N. The healing of oxygen vacancies in TiO_2 may be the reason for the increase in R_N at high T and exposure to high O_2 concentrations [39]. This process is inertial and, consequently, manifested during prolonged testing of samples. To further stabilize the gas-sensitive properties of the films, doping with metal additives should be applied [40].

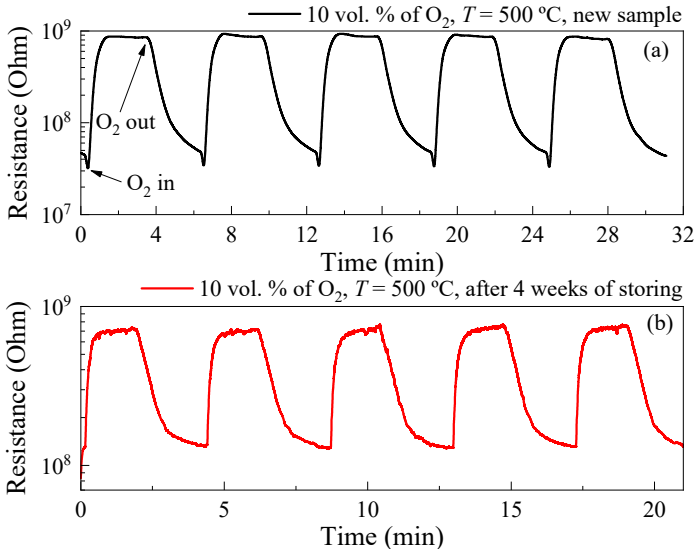

Figure 7. Time dependence of resistance upon cyclic exposure to 10 vol. % of O_2 at T = 500 °C for new sample (**a**) and after 4 weeks of storing (**b**).

The rise of resistance R of the TiO_2 thin film under the exposure to O_2 and the drop of resistance after this exposure were approximated by the following functions, respectively:

$$R(t) = R^{st}{}_{ox} - A \times \exp[-t/\tau_1], \quad (2)$$

$$R(t) = R^{st}{}_{N} + B \times \exp[-t/\tau_2], \quad (3)$$

where t is time; $R^{st}{}_{ox}$ is the stationary resistance of TiO_2 thin films in a gas mixture of dry N_2 + dry O_2; $R^{st}{}_{N}$ is the stationary resistance of TiO_2 thin films in dry N_2 atmosphere; A and B are constants; τ_1 and τ_2 are time constants. $\tau_1 \approx 23$ s and $\tau_2 \approx 25$ s at T = 500 °C and exposure to 10 vol. % of O_2 for new samples, $\tau_1 \approx 13$ s and $\tau_2 \approx 23$ s for samples after 4 weeks of storing. The time constants τ_1 and τ_2 are related to the relaxation times of adsorption and desorption of oxygen molecules on the semiconductor surface.

Figure 8a illustrates the time dependence of resistance of TiO_2 thin films at T = 500 °C and stepwise increase in the O_2 concentration c_{ox} (Figure 8b). The dependences of the response of TiO_2 thin films on c_{ox} at T = 500 °C in dynamic range from 0.1 vol. % to 100 vol. % of O_2 and 0.1 vol. % to 6 vol. % of O_2 are presented in Figure 8c,d, correspondingly. The samples demonstrate a wide dynamic range from 0.1 vol. % to 100 vol. % of O_2, but their responses to c_{ox} < 1 vol. % are low. Detailed research is needed to enhance oxygen sensitivity at these low oxygen concentration ranges.

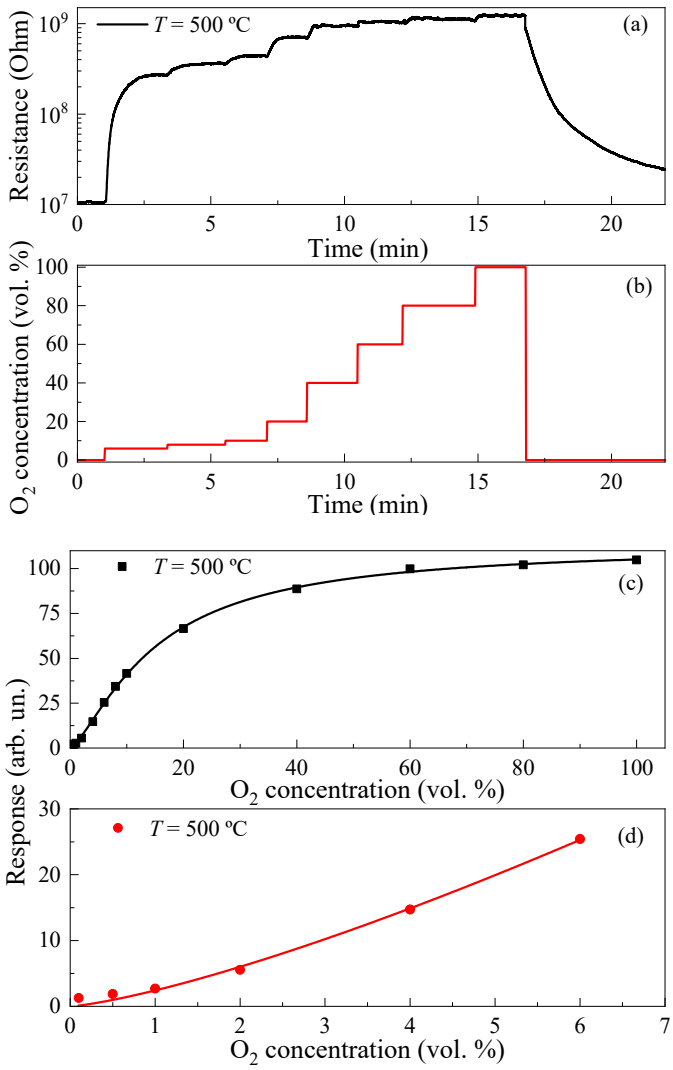

Figure 8. (**a**) Time dependence of resistance under stepwise increase in the O_2 concentration at T = 500 °C; (**b**) Time profile of O_2 concentration changes; (**c**) dependence of response on O_2 concentration in dynamic range from 0.1 vol. % to 100 vol. % of O_2 at T = 500 °C; (**d**) dependence of response on O_2 concentration in dynamic range from 0.1 vol. % to 6 vol. % of O_2 at T = 500 °C.

The effect of applied voltage on the response of TiO_2 thin films to O_2 was evaluated. The I–V characteristics of the samples were measured in dry N_2 atmosphere and in a dry gas mixture of N_2 + 10 vol. % of O_2 (shown in Figure 9a). The I–V characteristics were approximated by the power function $I \sim U^z$, where I is the electric current; z is a power index. The z value was 2.62 ± 0.05 in the N_2 atmosphere and 2.22 ± 0.05 in the gas mixture of N_2 + 10 vol. % of O_2. The nonlinearity of the I–V characteristics was probably caused by the manifestation of an energy barrier at the Pt/TiO_2 interface. The response of TiO_2 thin films to O_2 in the range of U = 0.2–1.5 V practically did not change with voltage (see Figure 9b). S_{ox} increased according to the power law $S_{ox} \sim U^k$ with the increase in U from 1.5 V to 5 V, where k is a power index. k was 0.62 ± 0.05 at c_{ox} = 10 vol. % and at T = 500 °C.

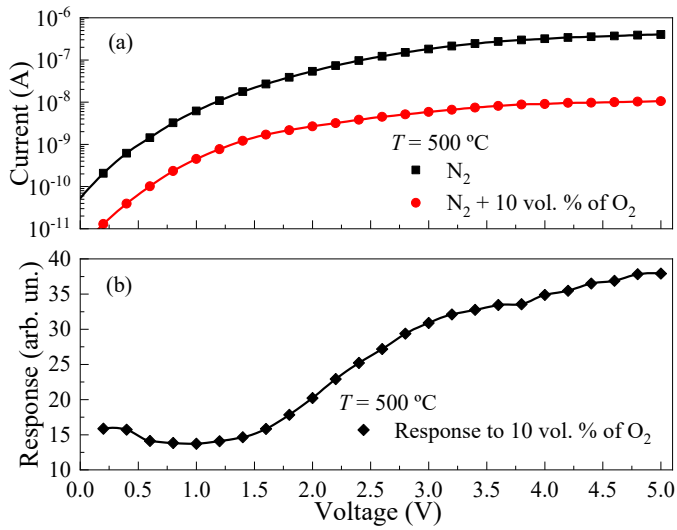

Figure 9. (**a**) *I*–*V* characteristics in N_2 atmosphere and gas mixture of N_2 + 10 vol. of O_2 at T = 500 °C; (**b**) dependencies of the responses to 10 vol. % of O_2 on applied voltage at T = 500 °C.

A promising application of O_2 sensors based on the ALD-TiO_2 thin films is the monitoring of the exhaust gases of the internal combustion engines. In order to achieve this, it is necessary to measure the change in O_2 concentration in the range of 6–10 vol. % in the exhaust gas mixture [2,41]. In addition to O_2, exhaust gases contain relatively high concentrations of H_2, NO_x, CH_x, CO and CO_2 [2,41,42]. To create a gas mixture corresponding to exhaust gas is difficult. But the sensitivity of the ALD-TiO_2 thin films to these gases with concentrations close to those of exhaust gases was investigated at the temperature of the maximum response to O_2. The ALD-TiO_2 thin films demonstrated a relatively high response to H_2, NO and NO_2. The experimental results are exhibited in Figure 10. The responses to relatively high concentrations of CO, CH_4 and CO_2 were insignificant or absent. Exposure to H_2 led to a drop in the resistance of the films. The ratio of resistances in the pure dry air and in the gas mixture of pure dry air + reducing gas (H_2, CO and CH_4) was chosen as response. The exposure to NO and NO_2 led to an increase in the TiO_2 thin film resistance. The response to these gases was determined as a ratio of the resistances in the gas mixture of pure dry air + NO (NO_2) and in the pure dry air. It is worth noting that the responses to 0.1 vol. % of H_2 and 7×10^{-4} vol. % of NO_2 were the same. This indicates the high sensitivity of the films to low NO_2 concentrations.

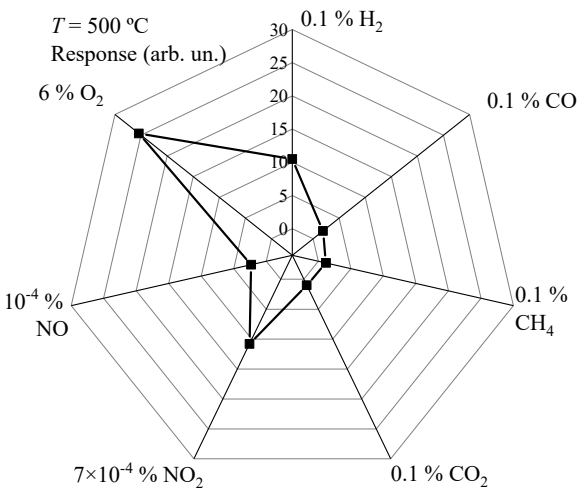

Figure 10. Responses to fixed concentrations of O_2, H_2, CO, CH_4, CO_2, NO_2 and NO at T = 500 °C.

3.3. The Mechanism of the Sensory Effect

The ALD-deposited TiO_2 thin films annealed at T_{ann} = 800 °C in Ar for 30 min are corresponding to the anatase phase. They are homogeneous and relatively smooth, without features of microrelief on the film surface which could affect the transport of charge carriers through the film. Therefore, the increase in the resistance of such TiO_2 films under exposure to oxygen is due to the chemisorption of O_2 molecules on their surface. During chemisorption, oxygen captures electrons from the TiO_2 conduction band and forms a region depleted by charge carriers in the near-surface part of the semiconductor film, with a width W. There are no charge carriers in this region, and the electric current between the contacts flows through a layer of thickness ($d - W$), which is called a conduction channel. The negative charge on the surface of the n-type semiconductor film leads to the formation of the upward bending of energy band eV_s, where vs. is the surface potential; e is the electron charge. It is shown that $eV_s \sim N_i^2$ [43,44], where N_i is the surface density of chemisorbed oxygen ions. The relationship between W and eV_s has the following form:

$$W = L_D \times [2eV_s/(kT)]^{0.5}, \quad (4)$$

where $L_D = [(\varepsilon\varepsilon_0 kT/(e^2 n)]^{0.5}$; k is the Boltzmann constant; ε is the electric constant. The chemisorption of oxygen on the surface of TiO_2 thin films leads to an increase in W and eV_s, as well as to a decrease in the thickness of the conduction channel that leads to an increase in the resistance of the film. At $n \approx 10^{18}$ cm^{-3}, L_D for the anatase TiO_2 phase increases linearly from 8.0 nm to 9.3 nm and does not exceed the film thickness. The TiO_2 film resistance in gas mixture $N_2 + O_2$ is given by

$$R_O = \rho_N l[b(d - W)], \quad (5)$$

where ρ_N is the resistivity of the TiO_2 film in the dry N_2 atmosphere; l is the distance between the electrodes; b is the width of the TiO_2 film. The intrinsic surface states can be neglected for ionic semiconductors [43]. Thus, in the N_2 atmosphere, eV_s and $W = 0$, and $R_N = \rho_N l/(bd)$. The expression for response to oxygen is

$$S_{ox} = (1 - W/d)^{-1}. \quad (6)$$

High S_{ox} takes place when the region depleted by charge carriers extends almost the entire thickness of the film, but there is a very thin conduction channel. The dependences of W and eV_s on T and c_{ox} (Figure 11a,b) are estimated by means of experimental S_{ox} and calculated L_D values. Pure TiO_2 thin films do not demonstrate reliably recorded sensitivity to O_2 at T < 450 °C. An increase in T stimulates dissociative adsorption of O_2 molecules. At the same time, high W and eV_s are observed in the range of T = 500–650 °C, indicating a high surface density of chemisorbed O^- ions. A further increase in T leads to a predominance of O^- desorption, which leads to a sharp decrease in W and eV_s, as well as the response of films. There are two linear areas on the dependencies of W and eV_s on the O_2 concentration in double logarithmic coordinates (Figure 11b). $eV_s \sim c_{ox}^{l_1}$ and $W \sim c_{ox}^{m_1}$ in the range of c_{ox} = 0.1–2 vol. %, where l_1 and m_1 are the power indexes. $l_1 = 0.90 \pm 0.03$ and $m_1 = 0.45 \pm 0.01$. The equality $m_1 = l_1/2$ follows from Expression (4). There are weaker power dependencies of $eV_s \sim c_{ox}^{l_2}$ and $W \sim c_{ox}^{m_2}$ in the range of c_{ox} = 4–100 vol. %, where l_2 and m_2 are the power indexes. At the same time, $l_2 = 0.028 \pm 0.006$ and $m_2 = 0.014 \pm 0.003$. We assume that the manifestation of two linear areas on the dependencies is due to the presence of two types of adsorption centers for oxygen molecules. The possibility of this was shown for SnO_2 and Ga_2O_3 thin films [45,46]. As a result, oxygen is chemisorbed in the form of O^{2-} on the first type of adsorption centers and in the form of O^- on the second one. Chemisorption on the centers of the first type prevails in the range of c_{ox} = 0.1–2 vol. %. Twice as many electrons are captured during the chemisorption of one oxygen molecule on this type of centers, which causes a sharp increase in W and eV_s. Centers of the second type prevail in the range of c_{ox} = 4–100 vol. % and the dependencies of W and eV_s on

c_{ox} are much weaker. In this case, $eV_s \sim (N_{i1} + N_{i2})^2$, where N_{i1} is the surface density of chemisorbed O^{2-} ions; N_{i2} is the surface density of chemisorbed O^- ions. It is worth noting that it is possible to approximate the experimental dependence of the response on the O_2 concentration (see Figure 8c) by means of Expressions (4) and (6) in the case when $eV_s(c_{ox}) = a(c_{ox}) \times c_{ox}^{l_{1,2}}$, where a is a function of c_{ox}. We believe that this dependence of $eV_s(c_{ox})$ is due to the manifestation of the dependence of the surface density of adsorption centers for oxygen molecules on c_{ox}.

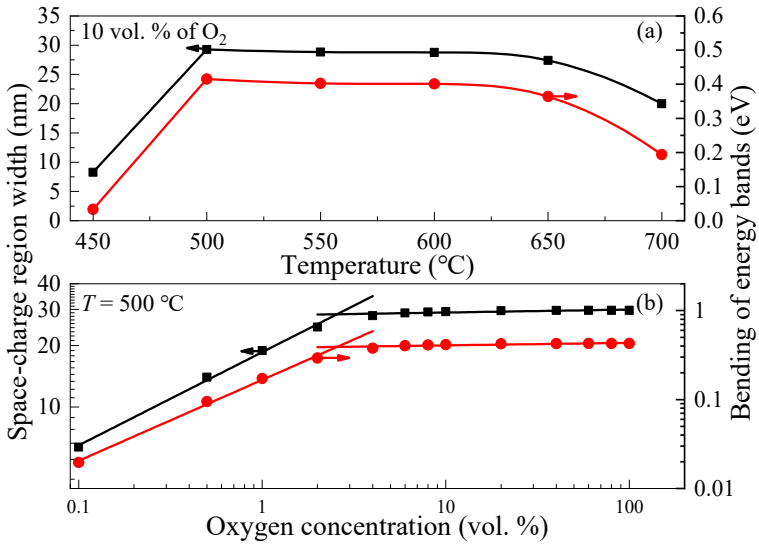

Figure 11. (**a**) Dependences of space-charge region width and bending of energy bands on temperature at c_{ox} = 10 vol. % of O_2; (**b**) dependences of space-charge region width and bending of energy bands on oxygen concentration at T = 500 °C.

The effect of applied voltage on the response of metal oxide to gases has been poorly studied in the literature so far. For SnO_2 films, it is shown that negatively charged ions of chemisorbed oxygen diffuse over the surface, participating in the transport of the electric current [47]. The diffusion time of adsorbed oxygen over the surface is less than its lifetime on the surface at high electric fields. Negatively charged ions accumulate near the anode and form a high-resistance region at higher electric fields. An additional increase in the resistance contributes to an increase in response at higher U.

Within the framework of the proposed mechanism of the sensory effect, the sensitivity of the films to reducing gases is due to the interaction of their molecules with previously chemisorbed oxygen, as a result of which W and eV_s, as well as the resistance of TiO_2 films, decrease. The mechanism of sensitivity of TiO_2 films to reducing gases was previously described in detail by our group in ref. [48]. Oxidizing gases interact with the surface of TiO_2 films like oxygen.

The proposed sensory effect does not take into account the contribution of changes in the potential barrier at the Pt/TiO_2 interface under the exposure to gases. The Schottky barrier between a semiconductor and catalytically active metals such as Pt, Pd, Ru, Ir, and Ag, including Pt/TiO_2 structures, are known to exhibit sensitivity to H_2 and other gases [38,49,50]. According to the corresponding sensory effect's mechanism, gas molecules (H_2 for example) undergo a dissociative adsorption on the catalytically active metal surface. Then, H atoms diffuse through the metal layer to the metal–semiconductor interface. A dipole layer of H atoms is formed at this interface, which leads to a decrease in the height of a potential barrier for electrons at the metal–semiconductor interface and an increase in the current. The diffusion of H atoms in Pt is characterized by lower diffusion activation energies and higher diffusion coefficients than those for the diffusion of O atoms in Pt [51–56]. It can be estimated that the diffusion times of H atoms through a 330 nm thick Pt layer are less than 0.055 s. In contrast, the diffusion time of O atoms through the Pt contact layer is about 10^8 s. Thus, changes in the potential barrier at the Pt/TiO_2 interface

under the exposure to O_2 should not be taken into account. However, this effect may be the main one under the exposure to other gases, such as H_2 and CO.

The gas-sensitive characteristics of TiO_2 films synthesized by different deposition methods under the exposure to O_2 are compared in Table 2, where NRA is nanorod array; NPs is the nanoparticles; NFs are the nanoflakelets; NTs is the nanotubes; RFMS is the radio frequency magnetron sputtering; DCMS is the direct current magnetron sputtering; IBSD is the ion beam sputtering deposition; GLAD + EBE is the glancing angle deposition with electron beam evaporation; AVO is the acid vapor oxidation; USP is the ultrasonic spray pyrolysis; TD + HM is the thermal decomposition assisted hydrothermal method; PEO is the plasma electrolytic oxidation; AO is the anodic oxidation; UV is the exposure to ultraviolet radiation. The gas-sensitive properties of ALD-deposited undoped TiO_2 thin films studied in this work are comparable or superior to the results reported for undoped TiO_2 thin films grown by other methods. High S_{ox} requires heating of the structures to $T > 300$ °C. T is reduced to RT by using of the ultrathin films or nanostructures, exposure to UV. However, at the same time, t_{res} and t_{rec} significantly increase. On the other hand, an increase in S_{ox} is achieved by doping of TiO_2 with Nb, Pd and Cr, introducing ZrO_2, MoO_3, forming of multilayer structures, and modifying the surface of films with nanoparticles.

Table 2. Comparison of sensitivity to O_2 for TiO_2 thin films deposited by different methods.

Material	Methods	d (nm)	c_{ox} (vol. %)	T (°C)	S_{ox} (arb. un.)	Ref.
TiO_2	RFMS	50	0.6	500	1.14	[18]
TiO_2	DCMS	60	10	*RT*	76	[5]
TiO_2	IBSD	130	40	750	7.64	[48]
TiO_2 Nb (6%):TiO_2	sol-gel	- -	2	700	6.5 73.2	[6]
TiO_2 TiO_2 + ZrO_2 (10 mol. %)	sol-gel	- -	1	400	4.4 5	[17]
TiO_2 Cr-TiO_2/TiO_2	RFMS GLAD + EBE	30 -	10	*RT* + UV	~5.5 ~9	[4]
TiO_2 NRA	AVO	-	8	*RT*	~1.9	[20]
TiO_2 TiO_2-Ag NPs	USP	- -	0.1	300	5 9	[57]
Pd:TiO_2	sol-gel	~110	1→20	240	1.27	[19]
TiO_2 TiO_2 + MoO_3 (25 at. %)	sol-gel	-	0.1	420 370	28 30	[58]
Au (6 nm)/TiO_2	RFMS	300	5	400	61.3	[59]
VO_x/TiO_2 NFs	TD + HM	-	0.01	500	1.32	[60]
Pt/TiO_2	PEO	-	10	*RT*	2	[61]
TiO_2 NTs	AO	-	4	100	160	[62]
TiO_2	sol-gel	-	4	252	1.16	[63]
TiO_2	ALD	23	0.1 1 2 10	500	1.27 2.70 5.55 41.61	This work

4. Conclusions

The structural and gas-sensitive properties under the exposure to O_2 within the temperature range from 30 °C to 700 °C of TiO_2 thin films deposited by atomic layer deposition on SiO_2/Si substrates were studied. The structure of the films annealed at 800 °C in an Ar for 30 min corresponded to the anatase phase. They are homogeneous and relatively smooth. The ALD-TiO_2 thin films demonstrated high responses to O_2 in the dynamic range from 0.1 to 100 vol. % and to low concentrations of H_2, NO_2. The greatest response—41.5 arb. un.—was observed at a temperature of 500 °C under exposure

to 10 vol. % of O_2. A mechanism describing the sensory effect in the ALD-TiO_2 thin films was proposed. The resistance of the films increases due to the chemisorption of oxygen molecules on their surface that decreases the thickness of the conduction channel between the metal contacts. It was suggested that there are two types of adsorption centers on the TiO_2 thin films surface: oxygen is chemisorbed in the form of O^{2-} on the first one and O^- on the second one.

Author Contributions: Conceptualization, A.V.A. and M.G.V.; methodology, N.N.Y., G.A.R. and K.I.L.; software, N.N.Y., G.A.R. and K.I.L.; validation, A.V.A.; formal analysis, A.V.A., M.G.V., G.A.R. and K.I.L.; investigation, N.N.Y., D.A.A., G.A.R. and K.I.L.; resources, A.V.A. and M.G.V.; data curation, A.V.A., D.A.A., M.G.V., G.A.R. and K.I.L.; writing—original draft preparation, A.V.A., D.A.A., M.G.V., G.A.R. and K.I.L.; writing—review and editing, A.V.A., D.A.A., M.G.V., G.A.R. and K.I.L.; visualization, A.V.A., M.G.V., G.A.R. and K.I.L.; supervision, A.V.A. and M.G.V.; project administration, A.V.A. and M.G.V.; funding acquisition, A.V.A. All authors have read and agreed to the published version of the manuscript.

Funding: Researches of gas-sensing properties of the ALD-deposited TiO_2 thin films were supported by the Russian Science Foundation, grant number 20-79-10043-P.

Data Availability Statement: Not applicable.

Conflicts of Interest: The authors declare no conflict of interest.

References

1. Kong, X.-H.; Wang, X.-F.; Liu, Q.-G. Research on oxygen sensor for metallurgical process. *J. Iron Steel Res. Int.* **2001**, *8*, 60–62.
2. Lampe, U.; Fleischer, M.; Meixner, H. Lambda measurement with Ga_2O_3. *Sens. Actuators B Chem.* **1994**, *17*, 187–196. [CrossRef]
3. Ramamoorthy, R.; Dutta, P.K.; Akbar, S.A. Oxygen sensors: Materials, methods, designs and applications. *J. Mater. Sci.* **2003**, *38*, 4271–4282. [CrossRef]
4. Jyothilal, H.; Shukla, G.; Walia, S.; Bharath, S.P.; Angappane, S. UV assisted room temperature oxygen sensors using titanium dioxide nanostructures. *Mater. Res. Bull.* **2021**, *140*, 111324. [CrossRef]
5. Wang, Y.; Lai, X.; Liu, B.; Chen, Y.; Lu, Y.; Wang, F.; Zhang, L. UV-induced desorption of oxygen at the TiO_2 surface for highly sensitive room temperature O_2 sensing. *J. Alloys Compd.* **2019**, *793*, 583–589. [CrossRef]
6. Gan, L.; Wu, C.; Tan, Y.; Chi, B.; Pu, J.; Jian, L. Oxygen sensing performance of Nb-doped TiO_2 thin film with porous structure. *J. Alloys Compd.* **2014**, *585*, 729–733. [CrossRef]
7. Polyakov, A.Y.; Smirnov, N.B.; Shchemerov, I.V.; Yakimov, E.B.; Pearton, S.J.; Ren, F.; Chernykh, A.V.; Gogova, D.; Kochkova, A.I. Electrical properties, deep trap and luminescence spectra in semi-insulating, Czochralski β-Ga_2O_3 (Mg). *ECS J. Solid State Sci. Technol.* **2019**, *8*, Q3019. [CrossRef]
8. Dimitrova, Z.; Gogova, D. On the structure, stress and optical properties of CVD tungsten oxide films. *Mater. Res. Bull.* **2005**, *40*, 333–340. [CrossRef]
9. Gogova, D.; Gesheva, K.; Kakanakova-Georgieva, A.; Surtchev, M. Investigation of the structure of tungsten oxide films obtained by chemical vapor deposition. *Eur. Phys. J. Appl. Phys.* **2000**, *11*, 167–174. [CrossRef]
10. Gogova, D.; Iossifova, A.; Ivanova, T.; Dimitrova, Z.; Gesheva, K. Electrochromic behavior in CVD grown tungsten oxide films. *J. Cryst. Growth* **1999**, *198–199*, 1230–1234. [CrossRef]
11. Kachel, K.; Korytov, M.; Gogova, D.; Galazka, Z.; Albrecht, M.; Zwierz, R.; Siche, D.; Golka, S.; Kwasniewski, A.; Schmidbauer, M.; et al. A new approach to free-standing GaN using β-Ga_2O_3 as a substrate. *CrystEngComm* **2012**, *14*, 8536–8540. [CrossRef]
12. Stolze, M.; Gogova, D.; Thomas, L.-K. Analogy for the maximum obtainable colouration between electrochromic, gaschromic, and electrocolouration in DC-sputtered thin WO_{3-y} films. *Thin Solid Films* **2005**, *476*, 185–189. [CrossRef]
13. Nikolskaya, A.; Okulich, E.; Korolev, D.; Stepanov, A.; Nikolichev, D.; Mikhaylov, A.; Tetelbaum, D.; Almaev, A.; Bolzan, C.A.; Buaczik, A., Jr.; et al. Ion implantation in β-Ga_2O_3: Physics and technology. *J. Vac. Sci. Technol. A* **2021**, *39*, 030802. [CrossRef]
14. Zappa, D.; Galstyan, V.; Kaur, N.; Hashitha, M.M.; Sisman, O.; Comini, E. Metal oxide -based heterostructures for gas sensors. *Anal. Chim. Acta* **2018**, *1039*, 1–23. [CrossRef]
15. Yakovlev, N.N.; Almaev, A.V.; Nikolaev, V.I.; Kushnarev, B.O.; Pechnikov, A.I.; Stepanov, S.I.; Chikiryaka, A.V.; Timashov, R.B.; Scheglov, M.P.; Butenko, P.N.; et al. Low-resistivity gas sensors based on the In_2O_3-Ga_2O_3 mixed compounds films. *Mater. Today Commun.* **2023**, *34*, 105241. [CrossRef]
16. Zhu, J.; Xu, Z.; Ha, S.; Li, D.; Zhang, K.; Zhang, H.; Feng, J. Gallium oxide for gas sensor applications: A comprehensive review. *Materials* **2022**, *15*, 7339. [CrossRef]
17. Mokrushin, A.S.; Simonenko, E.P.; Simonenko, N.P.; Bukunov, K.A.; Gorobtsov, P.Y.; Sevastyanov, V.G.; Kuznetsov, N.T. Gas-sensing properties of nanostructured $TiO_{2-x}ZrO_2$ thin films obtained by the sol–gel method. *J. Sol.-Gel. Sci. Technol.* **2019**, *92*, 415–426. [CrossRef]

18. Lu, C.; Huang, Y.; Huang, J.; Chang, C.; Wu, S. A Macroporous TiO_2 oxygen sensor fabricated using anodic aluminium oxide as an etching mask. *Sensors* **2010**, *10*, 670–683. [CrossRef]
19. Wang, H.; Chen, L.; Wang, J.; Sun, Q.; Zhao, Y. A micro oxygen sensor based on a nano sol-gel TiO_2 thin film. *Sensors* **2014**, *14*, 16423–16433. [CrossRef]
20. Wang, H.; Sun, Q.; Yao, Y.; Li, Y.; Wang, J.; Chen, L. A micro sensor based on TiO_2 nanorod arrays for the detection of oxygen at room temperature. *Ceram. Int.* **2016**, *42*, 8565–8571. [CrossRef]
21. Wilson, R.L.; Simion, C.E.; Blackman, C.S.; Carmalt, C.J.; Stanoiu, A.; Di Maggio, F.; Covington, J.A. The effect of film thickness on the gas sensing properties of ultra-thin TiO_2 films deposited by atomic layer deposition. *Sensors* **2018**, *18*, 735. [CrossRef] [PubMed]
22. Du, X.; George, S.M. Thickness dependence of sensor response for CO gas sensing by tin oxide films grown using atomic layer deposition. *Sens. Actuators B Chem.* **2008**, *135*, 152–160. [CrossRef]
23. Marichy, C.; Donato, N.; Latino, M.; Willinger, M.G.; Tessonnier, J.-P.; Neri, G.; Pinna, N. Gas sensing properties and *p*-type response of ALD TiO_2 coated carbon nanotubes. *Nanotechnology* **2015**, *26*, 024004. [CrossRef] [PubMed]
24. Niskanen, A.J.; Varpula, A.; Utriainen, M.; Natarajan, G.; Cameron, D.C.; Novikov, S.; Airaksinen, V.-M.; Sinkkonen, J.; Franssila, S. Atomic layer deposition of tin dioxide sensing film in microhotplate gas sensors. *Sens. Actuators B Chem.* **2010**, *148*, 227–232. [CrossRef]
25. Rosental, A.; Tarre, A.; Gerst, A.; Sundqvist, J.; Hårsta, A.; Aidla, A.; Aarik, J.; Sammelselg, V.; Uustare, T. Gas sensing properties of epitaxial SnO_2 thin films prepared by atomic layer deposition. *Sens. Actuators B Chem.* **2003**, *93*, 552–555. [CrossRef]
26. Wei, Z.; Akbari, M.K.; Hai, Z.; Ramachandran, R.K.; Detavernier, C.; Verpoort, F.; Kats, E.; Xu, H.; Hu, J.; Zhuiykov, S. Ultra-thin sub-10 nm Ga_2O_3-WO_3 heterostructures developed by atomic layer deposition for sensitive and selective C_2H_5OH detection on ppm level. *Sens. Actuators B Chem.* **2019**, *287*, 147–156. [CrossRef]
27. Kim, D.H.; Kim, W.-S.; Lee, S.B.; Hong, S.-H. Gas sensing properties in epitaxial SnO_2 films grown on TiO_2 single crystals with various orientations. *Sens. Actuators B Chem.* **2010**, *147*, 653–659. [CrossRef]
28. Lee, J.-H.; Mirzaei, A.; Kim, J.-H.; Kim, J.-Y.; Nasriddinov, A.F.; Rumyantseva, M.N.; Kim, H.W.; Kim, S.S. Gas-sensing behaviors of TiO_2-layer-modified SnO_2 quantum dots in self-heating mode and effects of the TiO_2 layer. *Sens. Actuators B Chem.* **2020**, *310*, 127870. [CrossRef]
29. Xu, H.; Akbari, M.K.; Wei, Z.; Hu, J.; Verpoort, F.; Zhuiykov, S. Plasma-induced sub-10 nm Au-SnO_2-In_2O_3 heterostructures fabricated by atomic layer deposition for highly sensitive ethanol detection on ppm level. *Appl. Surf. Sci.* **2021**, *563*, 150400. [CrossRef]
30. Eadi, S.B.; Shin, H.J.; Song, K.W.; Choi, H.W.; Kim, S.H.; Lee, H.D. Development of ultrasensitive indium oxide layer with high response to NO_2 gas in indium gallium zinc oxide stack structure using atomic layer deposition. *Mater. Lett.* **2021**, *297*, 129943. [CrossRef]
31. Lou, C.; Yang, C.; Zheng, W.; Liu, X.; Zhang, J. Atomic layer deposition of ZnO on SnO_2 nanospheres for enhanced formaldehyde detection. *Sens. Actuators B Chem.* **2021**, *329*, 129218. [CrossRef]
32. Lou, C.; Huang, Q.; Li, Z.; Lei, G.; Liu, X.; Zhang, J. Fe_2O_3-sensitized SnO_2 nanosheets via atomic layer deposition for sensitive formaldehyde detection. *Sens. Actuators B Chem.* **2021**, *345*, 130429. [CrossRef]
33. Yeh, Y.-M.; Chang, S.-J.; Wang, P.-H.; Hsueh, T.-J. A TSV-structured room temperature *p*-Type TiO_2 nitric oxide gas sensor. *Appl. Sci.* **2022**, *12*, 9946. [CrossRef]
34. Kuo, C.-G.; Chen, J.-H.; Chao, Y.-C.; Chen, P.-L. Fabrication of a P3HT-ZnO nanowires gas sensor detecting ammonia gas. *Sensors* **2018**, *18*, 37. [CrossRef]
35. Bukauskas, V.; Olekas, A.; Senulien, D.; Strazdien, V.; Šetkus, A.; Kaciulis, S.; Pandolfi, L. Effect of thickness of ultra-thin tin oxide film based gas sensors. *Lith. J. Phys.* **2007**, *47*, 475–483. [CrossRef]
36. Kozhushner, M.A.; Bodneva, V.L.; Trakhtenberg, L.I. Sensor effect theory for the detection of reducing gases. *Rus. J. Phys. Chem. A* **2012**, *86*, 1281–1287. [CrossRef]
37. Ikim, M.I.; Gromov, V.F.; Gerasimov, G.N.; Spiridonova, E.Y.; Erofeeva, A.R.; Kurmangaleev, K.S.; Polunin, K.S.; Ilegbusi, O.J.; Trakhtenberg, L.I. Structure, conductivity, and sensor properties of nanosized ZnO-In_2O_3 composites: Influence of synthesis method. *Micromachines* **2023**, *14*, 1685. [CrossRef]
38. Almaev, A.V.; Nikolaev, V.I.; Yakovlev, N.N.; Butenko, P.N.; Stepanov, S.I.; Pechnikov, A.I.; Scheglov, M.P.; Chernikov, E.V. Hydrogen sensors based on Pt/α-Ga_2O_3:Sn/Pt structures. *Sens. Actuators B Chem.* **2022**, *364*, 131904. [CrossRef]
39. Bulyarskiy, S.; Koiva, D.; Gusarov, S.; Latipov, E.; Rudakov, G.; Svetukhin, V. Crystallization of amorphous titanium oxide films upon annealing in an oxygen atmosphere. *Mater. Sci. Eng. B* **2022**, *283*, 115802. [CrossRef]
40. Maksimova, N.K.; Almaev, A.V.; Sevastyanov, E.Y.; Potekaev, A.I.; Chernikov, E.V.; Sergeychenko, N.V.; Korusenko, P.M.; Nesov, S.N. Effect of additives Ag and rare-earth elements Y and Sc on the properties of hydrogen sensors based on thin SnO_2 films during long-term testing. *Coatings* **2019**, *9*, 423. [CrossRef]
41. Meixner, H.; Lampe, U.; Gerblinger, J.; Fleischer, M. Chemosensors for motor management systems of the future. *Fresenius' J. Anal. Chem.* **1994**, *348*, 536–541. [CrossRef]
42. Baranzahi, A.; Spetz, A.L.; Glavmo, M.; Carlsson, C.; Nytomt, J.; Salomonsson, P.; Jobson, E.; Häggendal, B.; Mårtensson, P.; Lundström, I. Response of metal-oxide-silicon carbide sensors to simulated and real exhaust gases. *Sens. Actuators B Chem.* **1997**, *43*, 52–59. [CrossRef]

43. Gaman, V.I. Physical principles of operation of oxidizing gas sensors based on metal oxide semiconductors. *Rus. Phys. J.* **2012**, *54*, 1364–1371. [CrossRef]
44. Simion, C.E.; Schipani, F.; Papadogianni, A.; Stanoiu, A.; Budde, M.; Oprea, A.; Weimar, U.; Bierwagen, O.; Barsan, N. Conductance model for single-crystalline/compact metal oxide gas-sensing layers in the nondegenerate limit: Example of epitaxial SnO_2(101). *ACS Sens.* **2019**, *4*, 2420–2428. [CrossRef] [PubMed]
45. Gaman, V.I.; Almaev, A.V.; Sevast'yanov, E.Y.; Maksimova, N.K. Influence of water vapors and hydrogen on the energy band bending in the SnO_2 microcrystals of polycrystalline tin dioxide films. *Rus. Phys. J.* **2015**, *58*, 179–187. [CrossRef]
46. Almaev, A.V.; Chernikov, E.V.; Novikov, V.V.; Kushnarev, B.O.; Yakovlev, N.N.; Chuprakova, E.V.; Oleinik, V.L.; Lozinskaya, A.D.; Gogova, D.S. Impact of Cr_2O_3 additives on the gas-sensitive properties of β-Ga_2O_3 thin films to oxygen, hydrogen, carbon monoxide, and toluene vapors. *J. Vac. Sci. Technol. A* **2021**, *39*, 023405. [CrossRef]
47. Simakov, V.V.; Yakusheva, O.V.; Grebennikov, A.I.; Kisin, V.V. Current-voltage characteristics of thin-film gas sensor structures based on tin dioxide. *Tech. Phys. Lett.* **2005**, *31*, 339. [CrossRef]
48. Almaev, A.V.; Yakovlev, N.N.; Kushnarev, B.O.; Kopyev, V.V.; Novikov, V.A.; Zinoviev, M.M.; Yudin, N.N.; Podzivalov, S.N.; Erzakova, N.N.; Chikiryaka, A.V.; et al. Gas sensitivity of IBSD deposited TiO_2 Thin Films. *Coatings* **2022**, *12*, 1565. [CrossRef]
49. Kwon, H.; Lee, Y.; Hwang, S.; Kim, J.K. Highly-sensitive H_2 sensor operating at room temperature using Pt/TiO_2 nanoscale Schottky contacts. *Sens. Actuators B Chem.* **2017**, *241*, 985–992. [CrossRef]
50. Schierbaum, K.D.; Kirner, U.K.; Geiger, J.F.; Göpel, W. Schottky-barrier and conductivity gas sensors based upon Pd/SnO_2 and Pt/TiO_2. *Sens. Actuators B Chem.* **1991**, *4*, 87–94. [CrossRef]
51. Ebisuzaki, Y.; Kass, W.J.; O'Keeffe, M. Solubility and diffusion of hydrogen and deuterium in platinum. *J. Chem. Phys.* **1968**, *49*, 3329–3332. [CrossRef]
52. Ishikawa, T.; McLellan, R.B. The diffusivity of hydrogen in the noble metals at low temperature. *Acta Metall.* **1985**, *33*, 1979–1985. [CrossRef]
53. Ferrin, P.; Kandoi, S.; Nilekar, A.; Mavrikakis, M. Hydrogen adsorption, absorption and diffusion on and in transition metal surfaces: A DFT study. *Surf. Sci.* **2012**, *606*, 679–689. [CrossRef]
54. Barth, J. Transport of adsorbates at metal surfaces: From thermal migration to hot precursors. *Surf. Sci. Rep.* **2000**, *40*, 75–149. [CrossRef]
55. Schmiedl, R.; Demuth, V.; Lahnor, P.; Godehardt, H.; Bodschwinna, Y.; Harder, C.; Hammer, L.; Strunk, H.; Schulz, M.; Heinz, K. Oxygen diffusion through thin Pt films on Si(100). *Appl. Phys. A* **1996**, *62*, 223–230. [CrossRef]
56. Velho, L.; Bartlett, R. Diffusivity and solubility of oxygen in platinum and Pt-Ni alloys. *Metall. Trans.* **1972**, *3*, 65–72. [CrossRef]
57. Castañeda, L.; López-Suárez, A.; Tiburcio-Silver, A. Influence of colloidal silver nanoparticles on the novel flower-like titanium dioxide oxygen sensor performances. *J. Nanosci. Nanotechnol.* **2010**, *10*, 1343–1348. [CrossRef]
58. Galatsis, K.; Li, Y.X.; Wlodarski, W.; Comini, E.; Faglia, G.; Sberveglieri, G. Semiconductor MoO_3–TiO_2 thin film gas sensors. *Sens. Actuators B Chem.* **2001**, *77*, 472–477. [CrossRef]
59. Jiao, M.; Zhao, X.; He, X.; Wang, G.; Zhang, W.; Rong, Q.; Nguyen, D. High-performance MEMS oxygen sensors based on Au/TiO_2 films. *Chemosensors* **2023**, *11*, 476. [CrossRef]
60. Raghu, A.V.; Karuppanan, K.K.; Pullithadathil, B. Highly Sensitive, Temperature-independent oxygen gas sensor based on anatase TiO_2 nanoparticle grafted, 2D mixed valent VO_x nanoflakelets. *ACS Sens.* **2018**, *3*, 1811–1821. [CrossRef]
61. Engelkamp, B.; Schierbaum, K. Oxygen sensing of Pt/PEO-TiO_2 in humid atmospheres at moderate temperatures. *Sensors* **2021**, *21*, 2558. [CrossRef] [PubMed]
62. Lu, H.F.; Li, F.; Liu, G.; Chen, Z.G.; Wang, D.W.; Fang, H.T.; Lu, G.Q.; Jiang, Z.H.; Cheng, H.M. Amorphous TiO_2 nanotube arrays for low-temperature oxygen sensors. *Nanotechnology* **2008**, *19*, 405504. [CrossRef] [PubMed]
63. Wang, H.; Wang, J.; Chen, L.; Yao, Y.; Sun, Q.; Qunming, Z. Integrated microoxygen sensor based on nanostructured TiO_2 thin films. *Micro Nano Lett.* **2015**, *10*, 597–602. [CrossRef]